Nearshore oblique sand bars

F. Ribas, A. Falqués, and A. Montoto

Departament de Física Aplicada, Universitat Politècnica de Catalunya, Barcelona, Spain

Received 18 May 2001; revised 15 October 2002; accepted 31 October 2002; published 15 April 2003.

[1] The coupling between hydrodynamics and the evolving topography in the surf zone has been theoretically examined for oblique wave incidence. It is shown that positive feedback can lead to the initial growth of several types of rhythmic systems of sand bars. The bars can be down-current oriented or up-current oriented, which means that the offshore end of the bar is shifted down-current or up-current with respect to the shore attachment. In the limit of strong current compared to wave orbital motion, very oblique down-current oriented bars are obtained with a spacing of several times the surf zone width. When wave orbital motions are dominant, systems of up-current oriented bars and crescentic/down-current oriented bars appear with spacings of the order of the surf zone width. The latter feature consists of alternating shoals and troughs at both sides of the break line with the inner shoals being bar-shaped and oblique to the coast. The growth (e-folding) time of the bars ranges from a few hours to a few days and it is favored by constant wave conditions. The range of model parameters leading to growth corresponds to intermediate beach states in between the fully dissipative and the fully reflective situations. Preliminary comparison with field observations shows qualitative agreement. *INDEX TERMS:* 4546 Oceanography: Physical: Nearshore processes; 4558 Oceanography: Physical: Sediment transport; 3210 Mathematical Geophysics: Modeling; 3230 Mathematical Geophysics: Numerical solutions; *KEYWORDS:* nearshore system, surf zone morphodynamics, rhythmic oblique sand bars, longshore sediment transport, stability analysis, self-organization mechanisms

Citation: Ribas, F., A. Falqués, and A. Montoto, Nearshore oblique sand bars, *J. Geophys. Res.*, *108*(C4), 3119, doi:10.1029/2001JC000985, 2003.

1. Introduction

[2] Nearshore sand bars appear very often in the surf and shoaling zones with an orientation parallel to the coast. One or two of them can occur and even more may coexist. The origin and migration of such bars are still open problems, although it is accepted that they are related to cross-shore sediment transport mechanisms [see, e.g., *Roelvink and Stive*, 1989; *Short*, 1999]. Nearshore bars may also have orientations oblique or perpendicular to the coast. Usually, such bars are attached to the coastline by a cusp and are spaced quite regularly along the coast. There is some confusion on the terminology. The term ''transverse or shore-normal bars'' sometimes refers to bars perpendicular to the coast or sometimes in a broader sense to bars which are not shore parallel. Since the present model results do not include bars exactly perpendicular to the coast, we will therein refer always to ''oblique bars,'' keeping in mind that the angle with the shore normal can range from large to very small values.

[3] The origin and dynamics of oblique bar systems are certainly intriguing and interesting from a scientific point of view. However, even more important is that these regular rhythmic patterns are a visible trace of simple physical mechanisms that may dominate the morphodynamics and hydrodynamics of the surf zone at large length scales. While shore parallel bars are a 2-dimensional (2D) phenomenon, oblique bars are essentially 3D morphological features. Thus it is obvious that their formation is necessarily related to the morphodynamics and hydrodynamics of the surf zone in plan view. In this respect, the processes responsible for their occurrence are expected to be distinct from those that form shore-parallel bars.

[4] Most of the experimental literature on nearshore sand bars has been devoted to shore-parallel bars, and so far little attention has been paid to oblique bars. Moreover, the various descriptions of oblique bars in the literature seem to deal with rather different types of bars, and it is difficult to state common characteristics of these features, even from a qualitative point of view. However, Table 1 presents some sites where oblique bar systems have been described, giving qualitative estimations of the hydrodynamics and the morphology. The corresponding references are also given.

[5] Oblique bars can occur both in open coasts and in closed environments (for instance lakes and bays) and their growth seems to be related to post-storm conditions. They can also be either subtidal or intertidal referring to whether the bars are permanently covered by water or if they are alternately submerged and exposed following the tidal cycle. Oblique bar systems are often observed in beaches with oblique wave incidence, so coexisting with longshore currents and they often migrate down-flow. Regarding the

0148-0227/03/2001JC000985

Table 1. Field Observations of Oblique Bar Systems[a]

Site[b]	Beach Type	Tides	Beach Slope	Longshore Bar	Spacing, m	Bar Orientation
1	Bay	intertidal	0.01	inexistent	~20	unknown
2	Open coast	intertidal	0.01	coexistent	~400	down-current
3	Open coast	subtidal	0.04	coexistent	12–180	unknown
3	Open coast	subtidal	0.02	coexistent	22–360	unknown
4	Lake	subtidal	0.03	inexistent	30–120	down-current
5	Open coast	intertidal	0.02	inexistent	90–760	down-current
6	Gulf	intertidal	0.002	inexistent	65–220	unknown
7	Gulf	intertidal	0.004	unknown	~50	unknown
8	Bay	unknown	0.001	unknown	~650	unknown
9	Open Coast	unknown	0.004	inexistent	200–530	up-current
10	Open Coast	intertidal	0.01	linked	100–300	down-current

[a]Qualitative description of some beaches where these rhythmic patterns are observed, with the corresponding references.

[b]Numbers correspond with the following beaches:

1. Trabucador beach, Ebro Delta, Mediterranean coast, Spain [*Falqués*, 1989].
2. Atlantic coast, France [*Guilcher et al.*, 1952; *Camenen and Larroude*, 1999].
3. Duck beach, Atlantic coast, U.S.A. [*Konicki and Holman*, 2000].
4. Lake Michigan, U.S.A. [*Evans*, 1938].
5. Several Oregon beaches, Pacific coast, U.S.A. [*Hunter et al.*, 1979].
6. St. James Island, Florida, Gulf coast, U.S.A. [*Niederoda and Tanner*, 1970].
7. Ochlockonee Point, Florida, Gulf coast, U.S.A. [*Barcilon and Lau*, 1973].
8. Bethany Beach, Delaware, U.S.A. [*Barcilon and Lau*, 1973].
9. Durras Beach, New South Wales, Australia [*Chappel and Eliot*, 1979].
10. New South Wales, Australia [*Wright and Short*, 1984; *Short*, 1999].

initial topography (before the growth of the features), these topographic systems appear in quite different beach profiles. They can be clearly linked to an existing shore-parallel bar, or coexist with longshore bars without a clear relationship with them, or also exist in places where there is no evidence of the presence of any shore-parallel bar.

[6] The alongshore bar spacing, λ, defined as the distance between the shore attachments, ranges from tens to hundreds of meters, i.e., the order of magnitude of the surf zone width, X_b. *Hino* [1974] reported observed spacings scattering between 3 and 8 times X_b, with a mean of 4 X_b. In analyzing several field data sets from the literature, *Falqués et al.* [1996] also found a relatively constant value of $\lambda \sim 1-6\ X_b$. Often, oblique bar systems are quasi-regular, which means that the spacing is not constant but shows quite large deviations from the mean value (see Table 1). The cross-shore span of the bars is usually of the same order or smaller than the surf zone width. The relationship between the bar orientation and the longshore current driven by the obliquely incident wave field is an open question. At some sites, the offshore end of the bar is shifted down-current with respect to the shore attachment, but it seems that the bars can orient themselves up-current too (site 9 in Table 1, for instance). In most cases, the hydrodynamics during the formation of the bars is not reported so that the bar orientation with respect to the longshore current is not known.

[7] In spite of the scarcity of systematic experimental data sets on oblique bars, some theoretical explanations for their existence have been given. *Holman and Bowen* [1982] showed how the superposition of two or more low-frequency edge waves of the same frequency but different mode number and wave length can generate a drift velocity pattern capable of forming oblique bars. However, the edge waves have to be "phase-locked," and the reason why this should be the case in nature is not clear (see discussion by *Falqués et al.* [1996]). Apart from the possibility that the hydrodynamic forcing by low-frequency edge waves may potentially play an important role in the origin of such bars, the importance of self-organization in the hydrodynamic and morphodynamic coupling should not be disregarded. A shoal in an otherwise alongshore uniform beach profile creates a certain nonuniformity in the wave breaking and current distribution. This modifies in turn the sediment transport pattern which may either damp or reinforce the shoal. In the latter case a positive feedback occurs between flow and morphology, and this is a potential source of topographic patterns. Any small topographic irregularity on the otherwise uniform situation can be expanded in the normal modes of the morphodynamic system so that it can potentially excite the most unstable mode (fastest growing mode) which may be a large regular pattern that eventually prevails. This provides an alternative explanation for the growth of oblique bars. Notwithstanding the potential role of low-frequency hydrodynamic forcing, these flow and morphology self-organization processes are active whenever sand, waves and currents interact.

[8] The hypothesis of a self-organization origin of nearshore oblique bars was first proposed by *Sonu* [1968]. *Barcilon and Lau* [1973] presented a first theoretical model where transverse bars stemmed from an instability of the longshore current due to the morphological coupling. This effect, whose corresponding physical mechanism is similar to the one leading to the growth of river bars (without wave effects), will be hereinafter referred to as "bed-flow" interaction. While that work was certainly pioneering, their results are invalidated by a mathematical error [*Falqués et al.*, 1993]. The initial approach of *Barcilon and Lau* [1973] was further pursued in a systematic way for the wave-driven longshore current by *Falqués et al.* [1996]. Several instability modes were found with $\lambda \sim 1-4\ X_b$. They can be described more appropriate as alternating shoals and troughs, reminiscent of alternate and multiple free bars in rivers, rather than nearshore oblique bars.

[9] However, the growing shoals in the surf zone do not produce only a deflection of the current but also a modification of the incident wave field (for instance, of the

breaking intensity). This effect, hereinafter referred to as "bed-surf" interaction, is usually mixed with the bed-flow coupling, but it can occur in isolation in case of wave incidence perpendicular to the coast. *Falqués et al.* [2000] and *Caballeria et al.* [2002] performed linear and nonlinear stability analysis (respectively) in case of normal-wave incidence. They showed that bed-surf interaction may result in the formation of crescentic patterns (alternating shoals and troughs at both sides of the mean break line) and of shore-normal bars.

[10] *Hino* [1974], the first to perform a morphodynamic stability study accounting for both bed-flow and bed-surf interactions, predicted the growth of shoals and troughs similar to oblique bars (down-current) with an alongshore spacing of about 4 X_b. In spite of the success of his model, the parameterizations of the wave field and sediment transport were not very realistic and the numerical solution procedure had a low resolution. *Christensen et al.* [1994] presented an instability analysis accounting for both bed-flow and bed-surf effects in much more realistic conditions and with a robust numerical solution procedure. Up-current oriented bars with a spacing of about 6 X_b were obtained. However, a number of aspects of this theoretical approach deserve further attention. First, the modeled bar orientation is at odds with the most often observed down-current orientation. Second, the results relied only on the dominant instability mode. Third, the physical origin of the instability was not investigated in depth. All the modeling studies mentioned above deal with instabilities of an equilibrium state with a monotone beach profile, i.e., without shore-parallel bars. A similar analysis was done in case of a longshore bar on the basic profile by *Deigaard et al.* [1999]. This paper predicted a modification of the longshore bar leading to a kind of crescentic feature, but it did not explain the growth of oblique bars.

[11] The present paper revisits the morphodynamic instability of a long rectilinear coast with an initially monotone beach profile (i.e., without longshore bars) in case of oblique wave incidence. The emphasis is now placed in an exploration of different sediment transport modes and in the physical mechanisms responsible for the growth of the bars. Another improvement with respect to the theory presented by *Christensen et al.* [1994] is that not only the dominant mode but the whole manifold of unstable modes are investigated for each case. This is very important with regard to a future nonlinear stability analysis or in case of an externally forced problem. In the work presented here both up-current and down-current oriented bars are obtained and a physical explanation for this behavior is given.

[12] Section 2 presents the theoretical setting of morphodynamic linear stability analysis. The corresponding numerical solutions are presented in section 3. The physical origin of the instability along with the reason for both possible orientations are investigated in section 4. A qualitative comparison with natural morphological patterns and other discussion points are addressed in section 5. The main overall conclusions are presented in section 6.

2. Theoretical Formulation

[13] A brief description of the theoretical formulation of our problem is given here. For further mathematical details see *Ribas et al.* [2000]. In this morphodynamic stability analysis we account for nearshore horizontal patterns growing from a reference topography which is alongshore uniform (see Figure 1). The y axis is chosen to coincide with the rectilinear coastline, the cross-shore and the vertical coordinates are x and z, running seaward and upward, respectively.

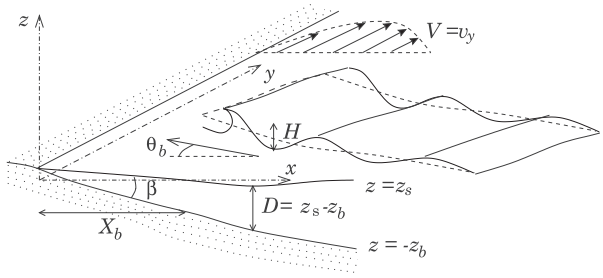

Figure 1. Coordinate system and basic state from which bedforms can grow due to instability. The dynamical system is the surf zone forced by obliquely incident waves. The basic state is characterized by uniform longshore flow, $v_y = V(x)$, free surface, z_s, and bottom surface, z_b, where the total depth is $D = z_s - z_b$.

[14] Fluid motions are based on the depth and wave averaged momentum and mass conservation [*Phillips*, 1977; *Horikawa*, 1988],

$$\frac{\partial v_i}{\partial t} + v_j \frac{\partial v_i}{\partial x_j} = -g\frac{\partial z_s}{\partial x_i} - \frac{\tau_{bi}}{\rho D} - \frac{1}{\rho D}\frac{\partial\left(\mathcal{S}'_{ij} - \mathcal{S}''_{ij}\right)}{\partial x_j} \qquad i = 1,2 \tag{1}$$

$$\frac{\partial D}{\partial t} + \frac{\partial\left(D v_j\right)}{\partial x_j} = 0, \tag{2}$$

where $\vec{v} = (v_1, v_2)$ is the depth averaged horizontal velocity, $x_1 = x$, $x_2 = y$ and repeated indexes are assumed to be summed. The gravitational acceleration is g, the mean free surface elevation z_s, the bed friction $\vec{\tau}_b$, the water density ρ and the total depth is $D = z_s - z_b$, where the sea bottom level is defined by $z = z_b(x)$. The wave radiation stress and the Reynolds turbulent stress tensors are $\mathcal{S}'$ and $\mathcal{S}''$, respectively. The morphological evolution is given by the sediment mass conservation equation,

$$\frac{\partial z_b}{\partial t} + \frac{\partial q_j}{\partial x_j} = 0, \tag{3}$$

where $\vec{q}(\vec{v}, z_b)$ is the horizontal sediment flux (cubic meters per meter and per second) divided by the porosity term. Parameterizations of small scale processes are needed in order to close the dynamical system. These are presented in the next subsections along with a description of the way to perform the linear stability analysis.

2.1. Waves, Bottom Friction and Turbulence

[15] The wave radiation stress, $\mathcal{S}'$, is computed from the linear wave theory,

$$\mathcal{S}'_{11} = E\left(\frac{c_g}{c}\left(1+\cos^2\theta\right)-\frac{1}{2}\right),$$

$$\mathcal{S}'_{22} = E\left(\frac{c_g}{c}\left(1+\sin^2\theta\right)-\frac{1}{2}\right), \quad (4)$$

$$\mathcal{S}'_{12} = -E\,\frac{c_g}{c}\cos\theta\sin\theta,$$

where $E = \frac{1}{8}\rho g H^2$ is the wave energy density, H is the wave height, θ is the wave incidence angle (between wave ray and the $-x$ axis) and c_g and c are the group and phase velocities, respectively. This study is mainly focused in isolating simple physical mechanisms that can lead to oblique bar formation. Thus, we are interested in using the simplest hydrodynamic description that can drive the sediment transport in a sensible way. To this end, a number of simplifications have been made on wave description: (1) shallow water wave kinematics, $c_g \simeq c \simeq \sqrt{gD}$, (2) small wave incidence angle, (3) regular waves and (4) saturated surf zone, $H = \gamma_b D$ (where γ_b is the breaking index), and wave forcing neglected out of the surf zone, $\partial \mathcal{S}'_{ij}/\partial x_j \simeq 0$. The validity of these assumptions will be examined in section 5.3. Using these simplifications, and taking Snell's law into account, the final expression for the wave radiation stress (equation (4)) becomes

$$\mathcal{S}'_{11} = \frac{3}{2}E,$$

$$\mathcal{S}'_{22} = \frac{1}{2}E,$$

$$\mathcal{S}'_{12} = -E\sqrt{\frac{D}{D_b}}\,\sin\theta_b,$$

where D_b and θ_b are the water depth and the incidence angle at the break point.

[16] Bottom shear stress is parameterized as being proportional to the mean flow through a coefficient which depends on the drag parameter, c_d, and the wave orbital velocity, u_o,

$$\tau_{b1} = \frac{4}{\pi}\,\rho\, c_d\, u_o\, v_1$$

$$\tau_{b2} = \frac{2}{\pi}\,\rho\, c_d\, u_o\, v_2.$$

This expression is met using the hypothesis of strong orbital velocity with respect to the mean currents and small wave incidence angle. The turbulent Reynolds stress is computed with the depth averaged eddy viscosity approach,

$$\mathcal{S}''_{ij} = \nu_t D\left(\frac{\partial v_i}{\partial x_j}+\frac{\partial v_j}{\partial x_i}\right), \quad i,j = 1,2$$

with a lateral mixing that is $\nu_t(x) = Nx\sqrt{gD}$ in the surf zone and has an exponential decay beyond the break line, where N is the turbulence parameter.

2.2. Equilibrium State

[17] The linear stability approach to the formation of bars by self-organization starts by defining a basic or reference state where bars are not present. This is an equilibrium (i.e., steady) and alongshore uniform state. The topography of the basic state is the equilibrium beach profile, $z_b = z_b^0(x)$, defined by the condition of zero cross-shore transport, $q_x(x) = 0$. We will here assume that this initial topography is a plane sloping beach, $z_b^0(x) = -\beta x$ (see Figure 1). The validity of this assumption will be discussed later on, in connection with the sediment transport parameterization chosen.

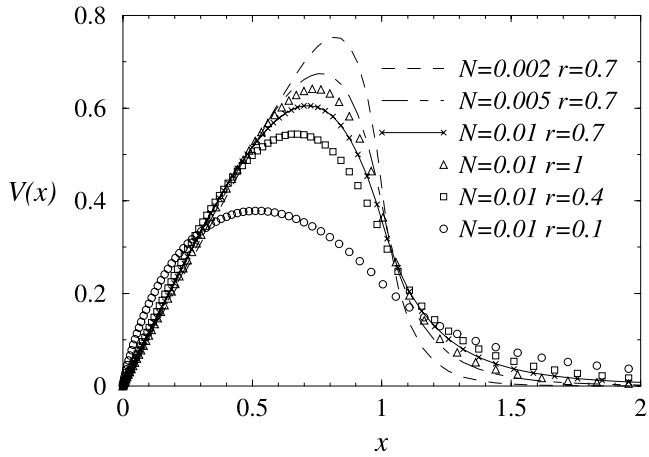

Figure 2. Effect of the bottom friction and the turbulence parameters (r, N) on the basic longshore current shape. All the variables are nondimensional, with $x = 1$ being the surf zone width and $V = 1$ being the maximum longshore current without turbulence.

[18] Obliquely incident waves generate a longshore current, $\vec{v} = (0, V(x))$, and an elevation of the mean free surface, $z_s = z_s^0(x)$. We have used the same parameterizations as *Longuet-Higgins* [1970] for the small-scale processes so that the equilibrium current is given by the analytical solution described in that paper. Figure 2 shows the dependence of the normalized longshore current, $V(x)$, on the bottom friction and the turbulence parameters. The obtained mean free surface elevation, $z_s^0(x)$, consists of a set-up inside the surf zone. Since wave forcing has been neglected out of the surf zone no set-down has been obtained there. Regular waves assumption leads to a single break point. The validity of such approximations will be analyzed in the Discussion (section 5.3).

2.3. Sediment Transport

[19] Equilibrium beach profile is supposed to come from a balance between the different cross-shore transport processes: wave asymmetry onshore transport, undertow offshore contribution, bound infragravity wave effects and down-slope gravitational transport [*Roelvink and Stive*, 1989]. Out of equilibrium, the dynamics of the cross-shore profiles (2D) is typically slower than the dynamics of the 3D features we pretend to describe [*Ruessink et al.*, 2000; *Plant et al.*, 2001]. This leads to the assumption that when alongshore inhomogeneities develop, the possible imbalance in the transport directly related to waves can be neglected in comparison with the transport driven by the longshore current and rip currents. This assumption essentially means that the 2D morphodynamics is frozen while

we look at the 3D one, which makes sense as long as both timescales are disparate.

[20] The sediment transport used in the present model is then proportional to the depth averaged current, $\vec{v}$. The transport related to a current in the presence of waves can be parameterized as a sum of terms of the form $\alpha_m(u_o)|\vec{v}|^{m-1}\vec{v}$ with several exponents m = (1, 3, 4), each one being dominant in different hydrodynamic conditions [see, e.g., *Bailard*, 1981]. The term α_m will be called "wave-stirring function" and depends on the wave orbital velocity, u_o. We use a sediment transport with the form

$$\vec{q}_m = \alpha_m(x)\ |\vec{v}|^m \left(\frac{\vec{v}}{|\vec{v}|} - \gamma\vec{\nabla}h\right), \tag{5}$$

instead of the sum, in order to get better insight into the different physical mechanisms governing under each hydrodynamic condition. The term $\gamma\vec{\nabla}h$, where $h = z_b(x, y, t) - z_b^0(x)$ is the deviation of the bottom level from the equilibrium profile, accounts for the tendency of the bottom irregularities to smooth out if they do not cause positive feedback into the flow. The coefficient γ is therefore called "morphodynamic diffusivity."

2.4. Linear Stability Analysis

[21] Equations (1), (2), and (3), together with the parameterizations used, define a dynamical system of four equations for the unknowns $\vec{v}$, z_s and z_b. Once the equilibrium or basic state has been computed, stability analysis can be applied in a standard way. A small perturbation assumed to be periodic in time and in the alongshore coordinate is added to this basic state,

$$(v_1, v_2, z_s, z_b) = \left(0, V(x), z_s^0, z_b^0\right) + e^{i(\kappa y - \omega t)}\,(u(x), v(x), \eta(x), h(x)). \tag{6}$$

The assumption of periodicity in the alongshore direction and of exponential dependence on time is not restrictive because, as the coefficients of the resulting linear system do not depend on y and t, any solution can be expanded as a sum or an integral of this type of solutions.

[22] By inserting equation (6) in the governing equations (1), (2), and (3), and linearizing with respect to the perturbations, we arrive at an eigenproblem for each κ. The eigenvalue is $\omega = \omega_r + i\omega_i$, and the eigenfunction is ($u(x)$, $v(x)$, $\eta(x)$, $h(x)$). The growth rate of the eigenfunctions is given by ω_i, so that $\omega_i > 0$ means growth. The migration celerity of the emerging bedforms is $c = \omega_r/\kappa$, where ω_r is the frequency. The alongshore spacing is $2\pi/\kappa$ and their shape is given by $\Re e\{e^{i\kappa y}h(x)\}$. In a similar way, the associated flow and the mean free surface elevation are obtained from $u(x)$, $v(x)$ and $\eta(x)$.

[23] In case of dealing with an unstable equilibrium state, some eigensolutions with a positive growth rate are found. The growth rate curves show these positive ω_i for different values of the wave number, κ. Hereinafter we will refer to each eigensolution as a "cross-shore mode" (or simply "mode"), the eigenfunction giving the cross-shore structure of the pattern and the eigenvalue indicating its dynamics. Several growing cross-shore modes can be obtained and they are referred to as modes [1, 2, 3, . . .], according to the maximum magnitude of their growth rate, from large to small. For each parameter setting, the pattern associated to the wave number with the maximum growth rate for the mode 1 (referred to as κ_M and ω_{iM}, respectively) will initially amplify the fastest and so it will determine the initial appearance of the beach and the dominant wave length. These are the eigenfunctions we will show by default. There can also be secondary modes that have different cross-shore structures than the dominant one.

[24] To first order in the developments, the perturbations in water depth due to the instability result in a perturbation of the break line position, because waves tend to break more over the growing shoals and less at the deepening troughs. This effect has been considered in the present paper so that the linearized governing equations consist not only of differential equations but also of integral-differential equations. A more detailed description of all this formulation is given by *Ribas et al.* [2000]. The refraction of the waves is only accounted for in the computation of the equilibrium state. The modifications of wave refraction due to bathymetric perturbations are neglected. The implications of this assumption are explained in section 5.3.

[25] Finally, a powerful tool to interpret the results of this linear stability analysis is the Flow Over Topography problem, hereinafter referred to as "FOT problem." This consists in solving only the three hydrodynamic equations for a given topographic perturbation h which is artificially fixed: that is, the sediment transport is switched off [*Falqués et al.*, 2000].

2.5. Scaling and Parameter Setting

[26] Before solving the eigenproblem, the variables are scaled to deal with nondimensional equations. In particular, the horizontal distances are scaled with the width of the surf zone, X_b, so that the nondimensional wave number has to be multiplied by $X_b{}^{-1}$. Fluid velocities are normalized with the maximum longshore current magnitude predicted by *Longuet-Higgins* [1970], $U \sim (\beta/c_d)\sqrt{gH_b}\,\sin\theta_b$. The growth time and the period of the bars are scaled with the morphological timescale T_m, which is obtained by setting to 1 the order of magnitude of all the terms in the topographic evolution equation (3). This gives $T_m = \beta X_b^2/Q$ where Q is the order of magnitude of the sediment transport flux ($m^2\ s^{-1}$). An estimate of T_m is given in Appendix A. The nondimensional ω must be multiplied by T_m^{-1} to obtain dimensional quantities. Normalized friction terms are controlled by the friction parameter $r = c_d/\beta$ instead of c_d.

[27] The numerical model has been run to explore the morphodynamic instability modes for different parameter settings. The wave incidence angle θ_b has been varied from 1° to 35°. Typical values of the drag coefficient for bottom friction and mean beach slope can be taken from the literature as being c_d = (0.0005 − 0.02) and β = (0.001 − 0.05) [see, e.g., *Dodd et al.* [1992]. This could give in principle a wide range for the friction parameter, $r = c_d/\beta$. Nevertheless, coarse sediment (large c_d) is normally related to steep beaches (large β). The result is that r can be considered to range only from 0.1 to 1. According to *Longuet-Higgins* [1970], the turbulence parameter is set to N = (0.001 − 0.01). The breaking index has been fixed to γ_b = 0.8 which is a common value for regular waves, as given by *Horikawa* [1988]. A default value γ = 1 has been

used for the morphodynamic diffusivity. Bailard's parameterization for bedload sediment transport gives $\gamma = (\tan \Phi_c)^{-1}$ where $\Phi_c \sim 45°$ is the angle of repose of the sediment. More variability can be expected in case of suspended load but typical values are also of the order of 1. Sensitivity analysis with respect to values ranging from 0.1 to 10 has been performed.

[28] Three different powers of the current in the sediment flux equation (5), m = (1, 3, 4), have been considered [*Bailard*, 1981]. In the limit of weak current with respect to wave orbital velocity, the term with the exponent $m = 1$ is dominant. The name "wave-dominated beaches" will hereinafter refer to this situation. The exponents $m = 3$ or $m = 4$ are representative of the strong current limit (with respect to wave orbital motion), for bedload and suspended load, respectively. This situation will be referred to as "current-dominated beaches." Two different parameterizations for the wave stirring function α have been used. As was found in case of normal wave incidence [*Falqués et al.*, 2000], the most relevant characteristic of the stirring function is whether the gradient of the quotient, α/D, where D is the total water depth, is directed shoreward (case a) or seaward (case b) inside the surf zone. This behavior is also corroborated by the results described in the present paper. This quotient, α/D, will be called "potential stirring." A shoreward directed potential stirring (case a) will be obtained from a uniform stirring function ($\alpha(x) = const.$) whereas a stirring increasing quadratically inside the surf zone ($\alpha(x) = D(x)^2$) and uniform beyond the break line will be representative of case b. No important differences are expected using other descriptions of α as long as α/D displays the two described behaviors. From a physical point of view, case b characterizes beaches dominated by wind/swell waves, so that the wave stirring is expected to increase seaward with the wave height up to the break line. For instance, Bailard's parameterization in case of suspended load predicts an α function increasing with $D^{3/2}$ so that α/D increases seaward. On the other hand, when there is a significant low frequency wave energy, there can be an associated wave stirring close to the coast. In this case, the α function would be more or less uniform in the cross-shore direction (case a).

3. Model Results

[29] Three different types of rhythmic patterns have been found: very oblique down-current oriented bars, up-current oriented bars and crescentic/down-current oriented bars. The key point that switch from one type of pattern to another is mainly the sediment transport mode (m and α). The wave incidence angle, θ_b, has also a noticeable effect on the results. Figure 3 summarizes the various topographic patterns obtained as a function of these parameters.

3.1. Very Oblique Down-Current Oriented Bars

[30] In case of current-dominated beaches (m = 3, 4) and for any stirring function, a system of very oblique down-current oriented bars with an orientation of about 80° with respect to the shore normal is obtained. The spacing is several times the surf zone width and this system appears for $\theta_b > 5°$. The typical growth rate and dispersion curves for the three fastest growing modes are shown in Figure 4. The topography and flow perturbations corresponding to the wave numbers with maximum growth rate for the two first modes can be seen in Figure 5. To see the real appearance of the beach, the basic state should be added (a linear sloping bottom and the basic longshore current). Then, the perturbations in the flow would cause a meandering and acceleration/deceleration of the longshore current. The sequence of modes corresponds to a structure of super-harmonics: The number of crests and troughs at any particular cross-shore section increases with the mode number. The whole pattern migrates downstream and it is almost nondispersive. The ratio between the period and the growth time is $2\pi\omega_i/\omega_r \sim 4$ so that the bars grow faster than they move.

[31] The obtained bedform shape is robust under changes of θ_b, r, N and γ. Only the maximum growth rate, ω_{iM}, the corresponding wave number, κ_M, and the migration celerity, c_M, depend on these parameters. Figure 6 shows the dependence of these three quantities on θ_b and r for the first mode. As can be seen, ω_{iM}, κ_M and c_M increase with r and θ_b. The number of secondary modes also increases with θ_b and r. The dependence of their characteristics upon these parameters is similar to that of the dominant mode. Figure 6 also shows that, in the studied range of parameters, κ_M goes from 1 to 3. This means that the alongshore spacing of the bars ranges from 2 to 6 times the surf zone width. The ω_{iM} goes from 0.1 to 1 and c_M is in between 0.1 and 0.5. All the quantities given in this subsection are nondimensional. The corresponding dimensional values will be discussed in section 5 after finding a reasonable estimate for the morphological timescale.

[32] The turbulence parameter, N, and the morphological diffusivity, γ, have a clear damping role on the instability. Increasing N smoothes the gradients in the horizontal current field that are coupled to this pattern (see Figure 5). However, the growth is never totally suppressed within the realistic range of values of N. In contrast, there is a critical value of γ above which the alongshore uniform beach is stable, $\gamma_c \simeq 3$. Another interesting finding is that, even though small values of the diffusive parameters give rise to quite long wave lengths of the topographic patterns, for $\gamma = 0$ or $N = 0$ there is still a dominant wave length (i.e., a maximum in the instability curve). This is in contrast with many morphodynamic stability studies [*Schielen et al.*, 1993; *Hulscher*, 1996; *Falqués et al.*, 1996; *Calvete et al.*, 2001] and in accordance with *Deigaard et al.* [1999]. It is interpreted as a result of including bed-surf interaction that was not taken into account in the former papers. A typical example of the flow structure coupled to the growth of these bars is shown in Figure 5. Strong gradients in the current field seem to be necessary, the longshore current decelerating at the crests of the bars and accelerating at the troughs. One may also observe the slight onshore deflection of the longshore current on the crests and the offshore deflection at the troughs.

3.2. Up-Current Oriented Bars

[33] In case of wave-dominated beaches ($m = 1$) the two different stirring functions lead to different solutions. A uniform stirring across the surf zone leads to the generation of up-current oriented bars with an orientation of about 50° with respect to the shore normal. They only exist if $\theta_b > 5°$ and their alongshore spacing is of the order of the surf zone width. The growth rate and dispersion curves are not shown

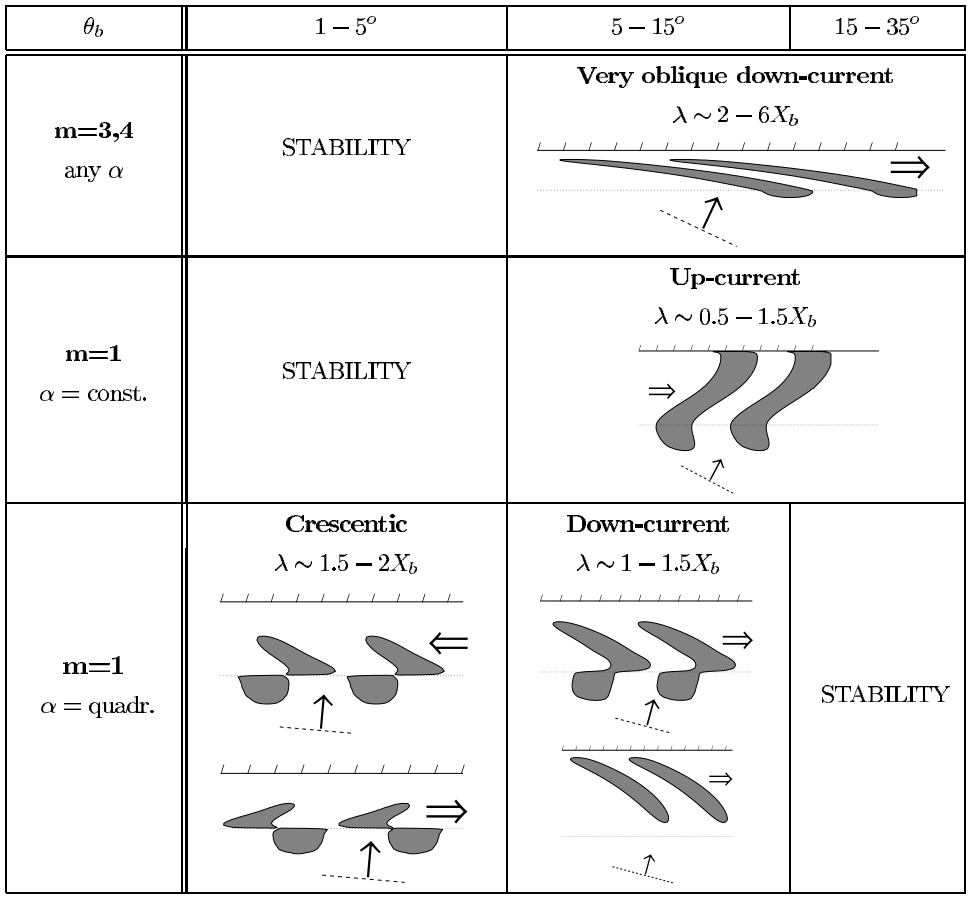

Figure 3. Summary of the different topographic features obtained as a function of the sediment transport mode and the wave incidence angle. In the pictures included in this table, the big double arrow indicates the direction of bar migration. The dashed line and the arrow perpendicular to it indicate the direction of wave incidence. The break line is represented with a pointed line parallel to the shoreline.

because the graphs are very similar to the ones shown in the subsection above (Figure 4), although now only one mode is obtained. The topography and flow perturbation patterns associated to this mode for the dominant wave number in a typical case are shown in Figure 7. The shape is reminiscent of the large-scale shoreface-connected sand ridges on the shelf, reported by *Calvete et al.* [2001]. A distinctive feature is a shoal that grows at the seaward end of each crest, probably due to the bed-surf interaction, which is obviously not relevant in case of the shelf ridges.

[34] Figure 8 shows the dependence of ω_{iM}, κ_M and c_M on r and θ_b for the first mode. When $\theta_b \to 0°$, ω_{iM} drops to zero quickly and κ_M tends to infinity. This is consistent with the fact that in case of $\theta_b = 0°$ instability was not found for this sediment transport mode [*Falqués et al.*, 2000]. On the other hand, for more oblique incidence ($\theta_b > 20°$), $\omega_{iM} \to 1$. The alongshore spacing ranges from 0.5 to 1.5 times the surf zone width, since κ_M goes from 4 to 12. The bars migrate downstream with a nondimensional celerity that increases in magnitude with θ_b. The topographic waves are nearly nondispersive (except for very large wave lengths). For the maximum amplified pattern, the ratio between the period and the growth time is $2\pi\omega_i/\omega_r \sim 1.6$. Now, the shape of the pattern is rather sensitive to r, specially because of the changes produced by this parameter in the longshore current profile. When r is small, the longshore current is smooth (see Figure 2) and the pattern grows close to the shore. Increasing r also increases slightly κ_M and c_M, whereas ω_{iM} decreases. Again, N and γ have a diffusive damping role. The flow pattern coupled to the growth of these bars is characterized by an offshore deflection of the

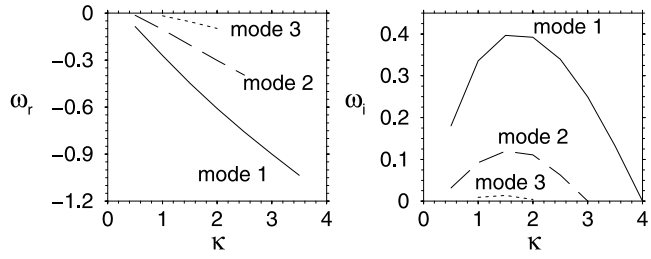

Figure 4. Dispersion line and growth rate curve for $m = 3$ and uniform α. Parameter values are: $\theta_b = 20°$, $r = 0.7$, $\gamma_b = 0.8$, $\gamma = 1$ and $N = 0.01$. All the variables are nondimensional. The values for the maximum growth rate, $\omega_{iM} = 0.40$, and the corresponding wave number, $\kappa_M = 1.75$ and frequency, $\omega_{rM} = -0.53$, of the first mode are extracted from this graph.

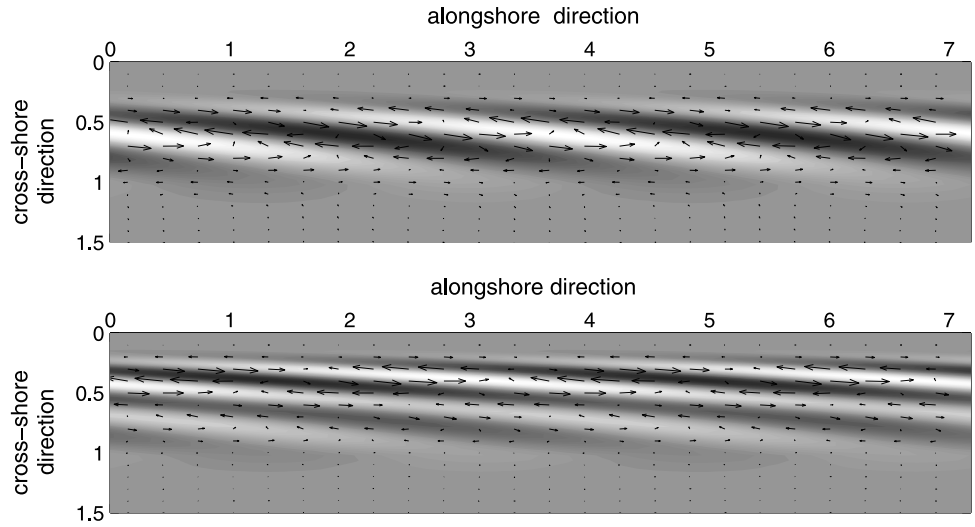

Figure 5. Very oblique down-current oriented bars. Topographic and current perturbations corresponding to the maximum wave number of mode 1 (Top) and mode 2 (Bottom) in case of $m = 3$ and uniform α. The alongshore direction is on the horizontal axis while the vertical axis is the cross-shore direction, running seaward. All the variables are non-dimensional, $x = 0$ being the coastline and $x = 1$ the break line. White areas correspond to crests and dark areas to pools. To see the real appearance of the beach, the basic state should be added (a linear sloping bottom and the basic longshore current). Waves come from the bottom left corner so the longshore current goes from left to right. Then, the perturbations in the flow would cause a meandering and acceleration/deceleration of the longshore current.

longshore current at the crests and an onshore deflection at the troughs.

3.3. Crescentic/Down-Current Oriented Bars

[35] Results are more rich in case of a stirring function increasing quadratically with the water depth from the shoreline up to the break line and constant beyond, which is also realistic in case of wave-dominated beaches ($m = 1$). There is instability only for incidence angles below some 10°–15°. When θ_b ranges from 3° to 15°, the fastest growing mode can be defined as alternating shoals and troughs at both sides of the break line with the inner shoals being bar-shaped and oblique to the coast. These inner bars are down-current oriented and the angle with the shore normal is some 60°. From now on we will refer to this solution as mode A1. Figure 9 shows the dispersion line and growth rate curve in case of $\theta_b = 5°$ and Figure 10 displays the topography and current perturbations of mode A1. The secondary mode (A2), can also be seen in both figures and consists of down-current oriented bars without any shoal out

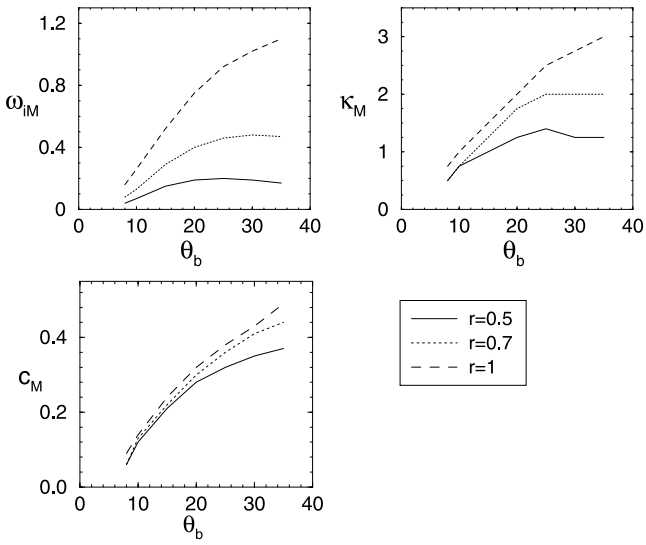

Figure 6. Effect of the wave incidence angle and the bottom friction on the maximum growth rate, wave number and migration celerity for $m = 3$ and uniform α.

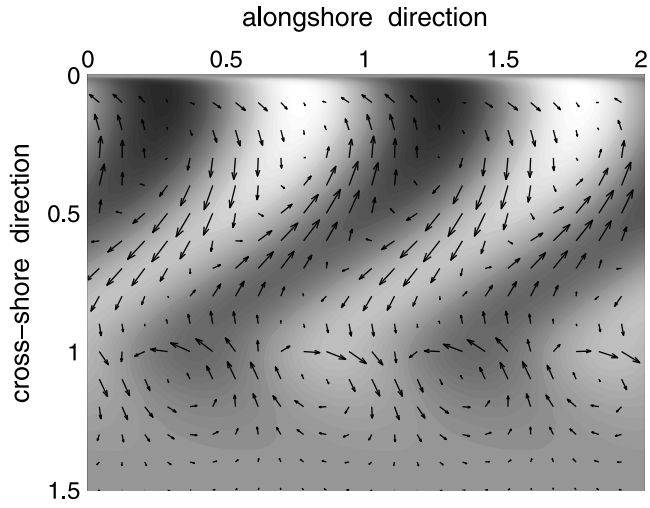

Figure 7. Up-current oriented bars. Topographic and current perturbations corresponding to the maximum wave number of the dominant mode in case of $m = 1$ and uniform α. The graph description is the same as in Figure 10.

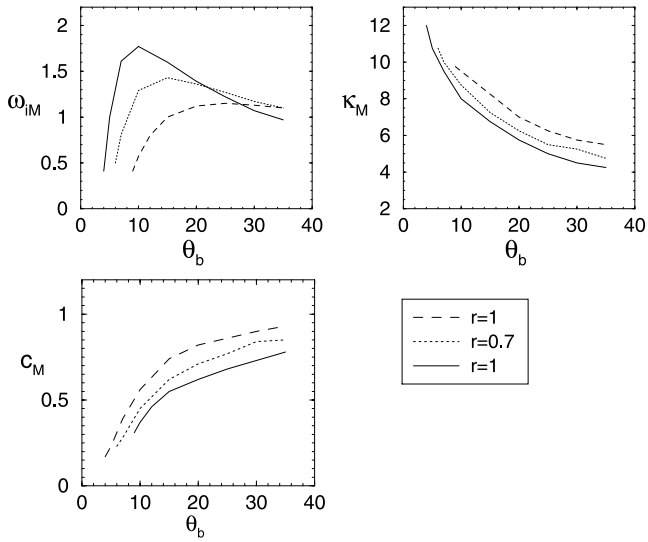

Figure 8. Effect of the wave incidence angle and the bottom friction on the maximum growth rate, wave number and migration celerity for $m = 1$ and uniform α.

of the surf zone (the angle with the shore normal being again some 60°). Its wave number is always larger than that of the first mode.

[36] Figure 11 shows the evolution of ω_{iM}, κ_M and c_M of the crescentic/down-current oriented feature (mode A1) as a function of θ_b and for several values of r. For $\theta_b > 5°$, the crescentic/down-current oriented bar system displays a constant wave number, $\kappa_M = 5$ and migrates slightly downflow ($c_M \simeq 0.5$). The alongshore spacing corresponding to this mode A1 is then some 1.5 times the surf zone width. Mode A2 displays smaller spacings of the order of the surf zone or smaller. When $\theta_b < 2°–3°$, mode A1 changes slightly the shape and another mode appears (denoted as mode B1). Both modes consists now of shoals at both sides of the surf zone and they migrate in opposite directions (mode A1 migrating upflow). A more detailed description of the results for very small incidence angle are given in Appendix B, together with a comparison with the results for $\theta_b = 0°$ (which were presented by *Falqués et al.* [2000]). The obtained bedform shape is very robust under changes in r, N and γ. These parameters have a clear damping role in these modes. The perturbed flow associated to these bedforms can also be seen in Figure 10. An onshore deflection of the current can be seen over the crests of the inner bars

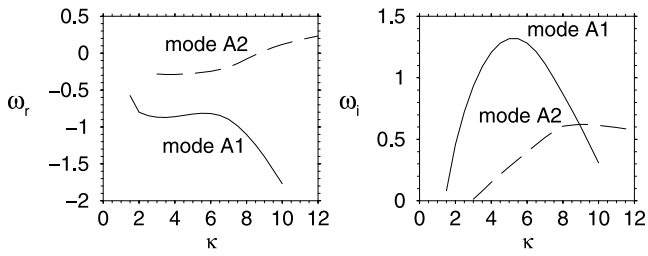

Figure 9. Dispersion line and growth rate curve for $m = 1$ and non-uniform $\alpha \sim D^2$. Parameter values are: $\theta_b = 5°$, $r = 0.5$, $\gamma_b = 0.8$, $\gamma = 1$ and $N = 0.01$. As it can be seen, $\kappa_M = 5.25$, $\omega_{iM} = 1.32$ and $\omega_{rM} = -0.82$.

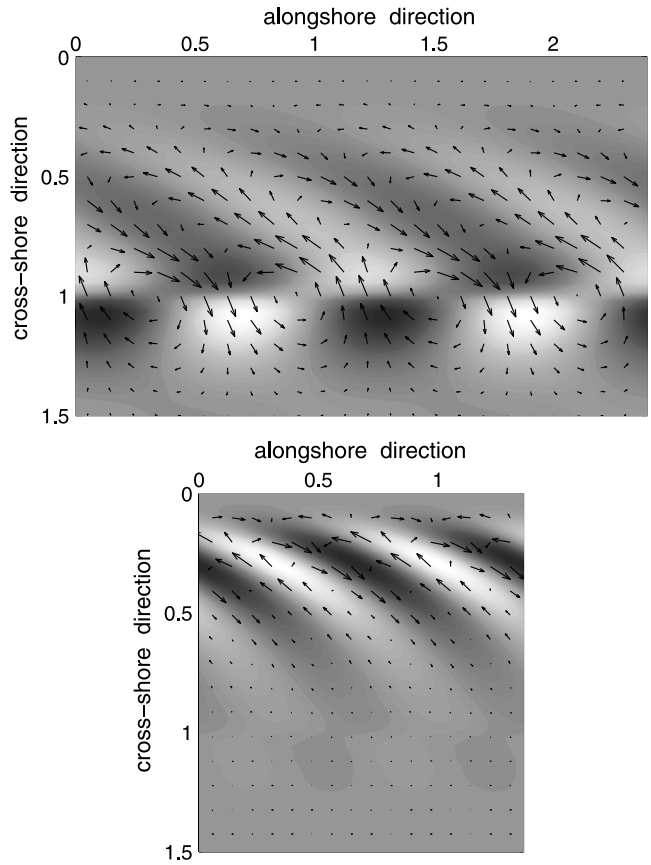

Figure 10. Crescentic/Downcurrent oriented bars. Topographic and current perturbations corresponding to the maximum wave number of mode A1 (Top) and mode A2 (Bottom) for $m = 1$, $\alpha \sim D^2$ and $\theta_b = 5°$. The graph description is the same as in Figure 10.

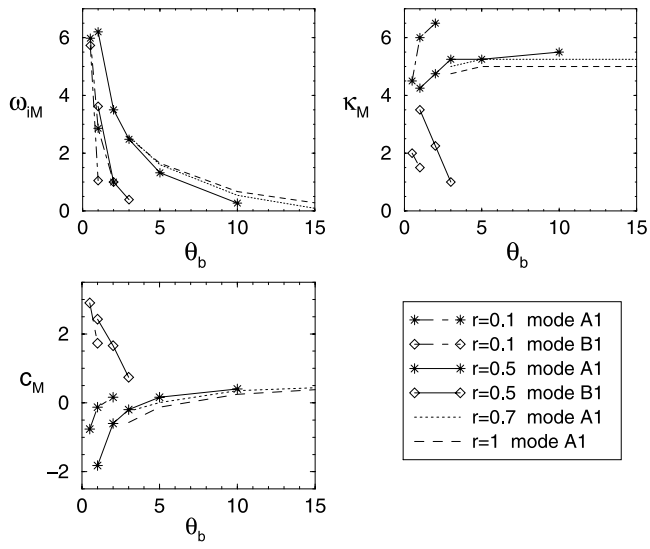

Figure 11. Effect of the wave incidence angle and the bottom friction on the maximum growth rate, wave number and migration celerity of modes A1 and B1 in case of $m = 1$ and $\alpha \sim D^2$.

and an offshore deflection occurs over the shoals out of the surf zone.

4. Physical Mechanisms

[37] The formation of the bars can be understood from a close examination of the interaction of the flow and the morphology. The morphological patterns that produce a flow structure causing accretion over the shoals and erosion at the troughs will grow. This requires two steps: (1) understanding the accretion/erosion pattern created by a particular flow and (2) understanding the flow caused by a given topography. Sections 4.1 and 4.2 present a first introduction to these two steps, respectively. Then this knowledge is applied to each particular type of bar in order to gain some insight into the generating physical mechanisms.

4.1. Bottom Evolution Equation

[38] The first step is accomplished by deriving a simple bottom evolution equation (BEE from now on) only from fluid and sediment mass conservation, complemented by the sediment transport parameterization we are considering. Inserting the transport formula equation (5) into the sediment conservation equation (3) and replacing $\nabla \cdot \vec{v}$ from the water mass conservation equation (2), results in

$$\frac{\partial h}{\partial t} - \frac{\partial}{\partial x_j}\left(\alpha\gamma|\vec{v}|^m \frac{\partial h}{\partial x_j}\right) = -(m-1)\alpha|\vec{v}|^{m-2} a_T - \alpha|\vec{v}|^{m-1}\vec{v}\nabla \ln\left(\frac{\alpha}{D}\right), \quad (7)$$

where $a_T = \vec{v} \cdot \nabla\vec{v} \cdot \vec{v}/|\vec{v}|$ is the tangential component of the advective acceleration of the fluid and repeated indices are implicitly summed over for $j = 1, 2$. The details of the derivation are given by *Caballeria et al.* [2002].

[39] The BEE can be linearized with respect to small perturbations superimposed to the equilibrium solution and thus reads

$$\frac{\partial h}{\partial t} + \frac{m\alpha V^m}{D_0}\frac{\partial h}{\partial y} - \frac{\partial}{\partial x_j}\left(\alpha\gamma V^m \frac{\partial h}{\partial x_j}\right) = \alpha V^{m-1}\left((m-1)\frac{\partial u}{\partial x_1} - \frac{\partial}{\partial x_1}\left(\ln\frac{\alpha V^{m-1}}{D_0^m}\right)u\right), \quad (8)$$

where an implicit addition over $j = 1, 2$ is again assumed and $(x_1, x_2) = (x, y)$. In absence of all the terms but the first two on the left-hand side, a first-order wave equation is obtained that describes the migration of bedforms along the coast with a local celerity $m\alpha V^m/D_0$. By adding the other term on the left-hand side, an advection-diffusion equation is obtained, with a diffusion coefficient $\alpha\gamma V^m$. Therefore, in absence of the terms on the right-hand side, the bedforms would in principle decay and migrate. Thus only the terms on the right can originate growth of the bedforms. A growing shoal needs $\partial h/\partial t > 0$ and, therefore, a positive right-hand side in equation (8).

[40] In accordance with equation (7), the first term in the right-hand side of equation (8) describes the effect of the acceleration of the flow. This term appears only in current-dominated beaches ($m > 1$), in which case $\alpha V^{m-1}(m-1) > 0$. So accretion occurs when $\partial u/\partial x > 0$. The second term in the right-hand side of equation (8) takes into account the gradients in the wave stirring, the water depth and the longshore current. This term produces accretion whenever the cross-shore component of the perturbation of the current, u, opposes the gradient in the function $\alpha V^{m-1}/D_0^m$. The physical interpretation of both terms will be better understood later on for each type of pattern.

4.2. Flow Over Topography Problem

[41] The second step of this theoretical analysis will be completed by understanding the flow caused by each kind of pattern in order to see if it is favorable to its growth. Some general properties of the flows generated by the different topographic patterns can be understood in terms of a competition between the bed-flow and the bed-surf effects. A ridge on an otherwise horizontal sea bed tends to deflect a current running obliquely through it in such a way that the current veers towards the normal to the crest as it runs over the ridge. This phenomenon, called "refraction of the current," can be explained as a consequence of water mass conservation and is essential for the generation of large-scale tidal sand banks [*Pattiaratchi and Collins*, 1987]. In case of nearshore bars, current refraction produces an offshore deflection of the current over up-current oriented bars (similarly to shoreface-connected sand ridges [*Calvete et al.*, 2001]) and an onshore deflection over down-current oriented bars.

[42] However, the hydrodynamics over surf zone oblique bars is not only governed by current refraction (bed-flow interaction) but also by the bed-surf interaction. In case of normal wave incidence, bed-surf effect tends to create onshore flow at the surf zone shoals (due to an increase in breaking) and offshore flow (rip currents) at the troughs between them [*Falqués et al.*, 2000; *Caballeria et al.*, 2002]. Nevertheless, the actual direction of the current if bed-surf effect dominates is very sensitive to the particular shape of the shoal because there are in fact two opposing hydrodynamic forces: an onshore force at the seaward part of the shoal (where breaking is increased by the increased bottom slope) and an offshore force at the shoreward part (where breaking is reduced by the reduced bottom slope). When wave incidence is oblique, new effects that are still not understood can take place.

4.3. Very Oblique Down-Current Oriented Bars

[43] In case of current-dominated beaches, (nonlinear sediment transport, $m = 3, 4$), both terms on the right-hand side of the linear BEE equation (8) are nonvanishing. The presence of both potentially destabilizing terms causes that the emerging type of bars cannot be predicted beforehand. Nevertheless, it is still possible to understand their formation once they are known as a model output.

[44] Instability turns out to be dominated by the acceleration term (proportional to $\partial u/\partial x$ in the linear BEE). Two reasons lead to this statement. Firstly, as shown in Figure 5, the flow pattern associated to these bars has strong gradients. If U is the scale for the cross-shore flow component, the term with $\partial u/\partial x$ in the BEE scales as $(m-1)\bar{\alpha}\bar{V}^{m-1}U/L_x$, where L_x, the typical distance associated to those gradients, is quite smaller than X_b. The term that is proportional to u scales as $\bar{\alpha}\bar{V}^{m-1}U/X_b$. Since $L_x \ll (m-1)X_b$, the

term proportional to $\partial u/\partial x$ becomes dominant. The second reason is that the term proportional to u has a stabilizing effect. The sign of the coefficient in front of u depends on whether $(\alpha/D_0)(V/D_0)^{m-1}$ is an increasing or a decreasing function. As α is kept constant, α/D_0 decreases seaward. A careful examination of the current distribution $V(x)$ for the Longuet-Higgins solution (see Figure 2) shows that $V(x)/D_0(x)$ is always a decreasing function. Therefore, $\alpha V^{m-1}/D_0^m$ is decreasing and, as a result, u must be positive to have growth. However, down-current oriented bars are predicted instead by the model with the corresponding onshore deflection of the current, $u < 0$ (caused by the bed-flow effect), so that this second term in equation (8) leads to a soft erosion of the pattern.

[45] The flow pattern coupled to the growing features (see Figure 5) clearly favors the instability generated by the acceleration term. The cross-shore component of the perturbation of the current, u, goes from negative to positive values when moving offshore across the bars. Thus, $\partial u/\partial x > 0$ over the crest of the bars and, therefore, the bars grow (since the coefficient in front of this derivative in equation (8) is always positive). The hydrodynamical effect that leads to this behavior of u remains unknown. Neither the bed-flow nor the bed-surf effect described in the subsection above can explain the acceleration of u over the crests. As quite oblique waves are necessary to the generation of such features, this acceleration is probably related with the radiation stress terms that depend on the wave incidence angle.

[46] Anyway, once the hydrodynamics is given as a result of the model, an interpretation of the physical mechanism can be made. The acceleration of u in the onshore direction is linked to a deceleration of v in the downflow direction due to the water mass conservation (this can be seen in Figure 5). The induced decrease of sediment carrying capacity in the downflow direction produces the accretion.

4.4. Up-Current Oriented Bars

[47] When dealing with wave-dominated beaches ($m = 1$) the situation is more simple (and hence more predictable) because the first right-hand side term of the linear BEE equation (8) vanishes and only the second one remains, leading to

$$\frac{\partial h}{\partial t} + \frac{\alpha V}{D_0}\frac{\partial h}{\partial y} - \frac{\partial}{\partial x_j}\left(\alpha\gamma V\frac{\partial h}{\partial x_j}\right) = -\alpha\frac{d}{dx}\left(\ln\frac{\alpha}{D_0}\right)u, \qquad (9)$$

where an implicit addition over $j = 1, 2$ is assumed. When a uniform wave stirring α is chosen, the α/D_0 function is decreasing offshore with the result that the coefficient in front of u is positive everywhere. Consequently, the growth of a shoal needs a seaward deflection of the current over it, $u > 0$ (and a shoreward deflection over the troughs). This type of flow is originated by current refraction over up-current oriented bars and so are the bedforms that appear in our model.

[48] The bed-surf interaction could also play a role in this pattern, specially in case of quite oblique wave incidence. For small wave incidence angle, it would tend to create onshore flow over the bars hence counteracting the current refraction. But it is also true that at the shoreward part of the bars the bed-surf force pushes the water seaward. Neither the net result of these opposing effects nor the influence of wave obliqueness is clear a priori. In order to understand the role of bed-surf interaction, the corresponding FOT problem has been solved. For arbitrary up-current oriented oblique bars, one may see that an onshore flow perturbation is generated by the bed-surf effect in case of small incidence angle (this inhibits the growth, as for the "giant cusp pattern" in the work by *Falqués et al.* [2000]). When waves approach the coast with larger angles ($\theta_b > 10°$), current refraction dominates generating the offshore flow over the crests that makes the bars grow. This causes that the features only appear above a critical angle of incidence. The formation of this type of bars is then certainly due to the bed-flow interaction.

[49] A physical interpretation of this instability can be made by decomposing the term given in equation (9) into two terms proportional to $-\vec{v}\cdot\nabla\alpha$ and to $\vec{v}\cdot\nabla D$, respectively. Since the sediment carrying capacity of the flow is proportional to α, a current running in the opposite direction of $\nabla\alpha$ (i.e., $-\vec{v}\cdot\nabla\alpha > 0$) produces a downstream decrease of sediment flux and, therefore, accretion occurs. A current running into deeper water (i.e., $\vec{v}\cdot\nabla D > 0$) slows down due to mass conservation (in fact, $\nabla\cdot\vec{v} < 0$). This causes a convergence of the sediment flux since it is proportional to a the flow velocity and, thereby, accretion takes place.

4.5. Crescentic/Down-Current Oriented Bars

[50] The last type of pattern is obtained in wave-dominated beaches with a nonuniform wave stirring, so an α/D_0 increasing from the shoreline to the break line and decreasing beyond. Thus the coefficient in front of u in the term equation (9) is negative in the surf zone and positive out of the surf zone. Consequently, the growth of a shoal in the surf zone needs onshore deflection of the current over it (and offshore deflection over the troughs). The contrary occurs for shoals and troughs out of the surf zone.

[51] As it was given by *Falqués et al.* [2000], this is the sort of circulation produced by the bed-surf effect over the crescentic patterns for normal wave incidence. For oblique incidence with a small angle until $\theta_b < 2-3°$, the longshore current is very weak so that bed-surf effect still dominates. The obtained bedforms (modes A1 and B1 in Appendix B) are similar to the two migrating crescentic patterns found for normal wave incidence [*Falqués et al.*, 2000]. Although the current is small, it breaks the symmetry and the non-migrating crescentic pattern that was obtained in that paper is now suppressed. The influence of the current increases with θ_b. As shown in Appendix B, the inner shoals of mode A1 are elongated with the shape of down-current oriented bars, while the contrary occurs for mode B1. Because current refraction produces onshore deflection over down-current oriented bars, mode A1 is favored by the current while mode B1 disappears for $\theta_b > 2°-3°$. At the troughs between the bars an offshore deflection of the current takes place. If the bars extend close to the break point (and this is so for the dominant mode, A1), this seaward flow crosses the break line and therefore, a shoal forms in front of the surf zone trough. Thus, a structure of surf zone bars with outer shoals in front of their troughs occurs. For θ_b up to $10°-15°$, the growth of these shoals is also favored by the bed-surf effect, but in case of larger angles, bed-surf is not dominant anymore and the structure disappears. The corre-

sponding physical mechanism is the one described in section 4.4.

5. Discussion

5.1. Comparison With Field Observations

[52] A quantitative comparison of the model results with field observations is not at all obvious considering the restrictions imposed by both the linearized analysis and the existing field data. The outputs of our linear stability analysis are the shape of the fastest growing mode, including its spacing, the growth time and the migration celerity. These results are only applicable at the beginning of the formation of the features. The main inputs of the model are the sediment transport mode, the wave incidence angle and the surf zone width during this initial stages of growth. All this information is largely lacking at most of the literature on field data (see Table 1) because it is difficult to know when bars start growing. The shape, spacing and celerity described in these sites correspond to the finite-amplitude features. Moreover, the hydrodynamics responsible for the growth is hardly ever given. In the sites where certain wave conditions are persistent, the available mean values for the surf zone width and the wave incidence angle can be used for comparison.

[53] Five different sites where hydrodynamic information is given have been used for a reasonable qualitative comparison with our theoretical predictions (see Table 2). The wave incidence angle far offshore, θ_∞, and the wave height at the break point, H_b, are shown in this table. Data are obtained either from the papers or from personal communication with the authors. As we have already remarked, these two parameters describing wave field have in general a large uncertainty. The incidence angle at the break point, θ_b, which is the one described in our model, is smaller than the angle reported in this table because of refraction when waves approach the break point. For instance, a typical wave of 8*s* period arriving at a water depth of 8*m* with an angle of $\theta = 30°$, is refracted to $\theta = 15°$ at 2*m* water depth (before breaking). The surf zone width has been estimated as $X_b = H_b/\beta\gamma_b$. The mean value of the observed spacing between bars, λ_e, is also shown along with the predicted spacing range from the model, λ_t. This latter quantity has been computed as the surf zone width times the nondimensional λ_t obtained from the model for the corresponding sediment transport mode, *m*.

[54] The Truc Vert (site 2) and Oregon (site 4) beaches are exposed to persistent Atlantic and Pacific obliquely incident swell. For instance, *Guilcher et al.* [1952] explain that an oblique wave incidence angle is essential for the growth of the bar systems in the French Atlantic Coast. These systems do not grow in the Southern part of this French coast, where the North Spanish coast is met, because the shoreline has another orientation so that the angle of incidence becomes much smaller (nearly normal wave incidence). The wave obliqueness is also remarked for the bars on the Lake Michigan (site 5). Therefore, the approximation of longshore current larger than wave orbital motion seems applicable (current-dominated beaches characterized by $m = 3, 4$ in our model). These three sites usually show persistent systems of very oblique down-current oriented bars with a spacing several times the corresponding surf zone width.

Table 2. Field Observations of Oblique Bar Systems[a]

Site[b]	Bar orientation	θ_∞	H_b	X_b	λ_e	λ_t	m
2	Down-current	27°	1.5	180	380	360–1000	3, 4
4	Down-current	30°	0.5	20	90	40–120	3, 4
5	Down-current	20°	1.5	90	300	180–540	3, 4
1	Unknown	-	0.25	30	20	15–45	1
3	Unknown	-	2	150	170	75–230	1
3	Unknown	-	1.5	50	80	25–80	1

[a]Representative values of the incidence angle far offshore, θ_∞, the wave height, H_b, the corresponding surf zone width, X_b, and a mean value of the experimental spacing of bar systems, λ_e. The predicted spacing range from the model, λ_t, together with the sediment transport mode used, *m*, are also shown. All the lengths are measured in meters.

[b]Numbers correspond with the sites shown in Table 1.

The rhythmic pattern obtained with our model for this sediment transport mode also has the same shape. As can be seen in Figure 3, predicted and observed spacings correlate well (although all the spacings are very different).

[55] One of the best described oblique bar systems for much more variable wave conditions is given by *Konicki and Holman* [2000] (site 3). These bars are secondary features to a pre-existing shore-parallel bar and grow both outside of the bar (offshore bars, exposed to large waves) or attached to the coast (trough bars, the energy has been reduced by the shore-parallel bar, last row in Table 2). They have an orientation of about 30–40° with respect to the shore normal. From the measurements presented in that paper, the orientation of the bars with respect to the longshore current cannot be known. The system of bars found in Trabucador Beach (site 1, which is facing the Alfacs Bay in the Ebro Delta, Spain) is also generated under variable wave conditions. Neither of these two sites show a preferred wave incidence angle so that comparison is more qualitative than in the first three sites. However, they might be related with wave-dominated beaches as wave incidence angles are usually not very large. They have then been compared with the case of $m = 1$. The corresponding bar systems have spacings of the order of X_b, in correlation with the predicted spacings. The crescentic/down-current oriented bar system obtained in our model reminds of the bar systems linked to a crescentic longshore bar described by *Wright and Short* [1984]. However, no quantitative data (along with hydrodynamics) have been found to compare with.

[56] Dimensional growth (e-folding) rates obtained are also in agreement with the experimental data. Field observations give guiding values of the order of 1 day [see, e.g., *Lippmann and Holman*, 1990]. The order of magnitude of the obtained morphological time ranges from a few hours to a few days (see Appendix A). This estimate of the growth time also provides a check on our basic assumption on sediment transport since this time is clearly smaller than the typical time of the 2D changes in the cross-shore beach profile given by *Plant et al.* [2001]. Guiding migration celerities are also reported in the literature. *Konicki and Holman* [2000] reported a variety of migration celerities ranging up to 40 m/day. Celerities from 5 to 10 m a day were observed at Oregon beaches [*Hunter et al.*, 1979] and about 1–2 m/day at Lake Michigan [*Evans*, 1938]. The velocities reported by *Konicki and Holman* [2000] refer only to the periods of time when the bars were active (significant wave energy). However, we do not know

whether this is so for the other two cases or if mean values for a large period of time were given there. According to equation (A4) in Appendix A, using $H_b \sim 1.5$ m and nondimensional celerities of $c \sim 0.2-0.6$, the predicted celerity for Duck is about 50 m/day which is not in disagreement with observations. In case of Oregon and Lake Michigan, the model results tend to overestimate the reported celerities by a factor about 20. This may be due to a number of reasons. First, the large uncertainty on the observed values already mentioned above. Also, the prediction of the model applies to the migration during the initial formation while the observed bars are already finite amplitude features. Finally, some uncertainty is also inherent in the estimate of the morphological time T_m, which affects the computation of the dimensional celerities.

5.2. Wave Conditions for Bar Growth

[57] The influence of the parameters of the model on the generation of bars has also been described in this paper. The question of which are the wave conditions conductive to the growth of rhythmic topography, which is a very relevant one, can be answered regarding the influence on the solutions of some parameters and assumptions. The discussion presented here is only qualitative since an accurate prediction of the influence of wave conditions is impossible without using more precise parameterizations of the small-scale processes.

[58] The morphodynamical diffusivity, γ, was able to set the transition from stability to instability in case of normal wave incidence [*Caballeria et al.*, 2002]. That paper predicted stability for very high values of the morphodynamic diffusion (corresponding to large waves) and growth of bar systems for lower values. The transition from stability to instability falling from very high wave energy to moderate energy is also found in case of oblique wave incidence. As an example, let us focus on the case $m = 4$, which is representative of current-dominated beaches. According to *Bailard* [1981], the current-driven transport scales as $|\vec{v}|^4$ while the downslope correction coefficient in front of ∇h scales as $|\vec{v}|^5/w_s$. Working out from those equations leads to the following formula for the morphodynamic diffusion,

$$\gamma \simeq 0.01 \frac{\beta \sin\theta_b}{c_d w_s} \sqrt{g H_b} \, . \tag{10}$$

The numerical threshold value above which there is stability is $\gamma_c \sim 3$ (section 3.1), from where a threshold value of $H_{bc} \sim 2$ m can be obtained for the wave height after assuming representative values of $c_d = 0.005$, $\beta = 0.01$, $\theta_b = 20°$ and $w_s = 0.01$ m s^{-1}. Thus, also in case of oblique wave incidence, very high energy would correspond to absence of alongshore rhythmicity in agreement to the "fully dissipative" state described by *Wright and Short* [1984]. The transition wave height of 2–3 m given in that paper is not in disagreement with our critical value $H_{bc} \sim 2$ m. It is also remarkable that all the oblique bar systems reported in Table 2 are observed for wave heights below 2 m. Finally it can be noted that decreasing sediment size leads to more dissipative states in the work of *Wright and Short* [1984], in agreement with the fact that, according to equation (10), small w_s and c_d leads to stability. Of course, low energy below the threshold for sediment transport would lead to stability too.

[59] Another important aspect of the occurrence of oblique bars in our model is that they need relatively fixed wave conditions during the time of growth, which ranges from a few hours to a few days. This is difficult to meet, especially during the beginning and the peak of a storm, but it is more likely for the swell period after the peak. So, oblique bars would form preferably in environments or during periods with relatively steady wave conditions. Also, the growth time is comparable or larger than the tidal period so the present study applies in principle only to micro-tidal beaches. How tidal oscillation can interfere with the mechanisms described here is still unknown from a theoretical point of view. Nevertheless, observations show that oblique bars certainly appear on meso-tidal conditions too [*Camenen and Larroude*, 1999]. This suggests that the mechanism described here is probably not inhibited by tidal variability.

[60] Looking at the consistency of the model hypothesis for each type of bar, very oblique down-current oriented bars grow for moderate incidence angle and strong current, which makes sense. Crescentic/down-current bars form under nearly normal incidence and weak current (with respect to wave orbital velocity), which is also consistent. However, up-current oriented bars grow for quite oblique wave incidence but weak current, which is not very likely.

5.3. Implications of the Model Assumptions

[61] In the basic equilibrium state, the waves are refracted as they approach to the coast obliquely. When small perturbations grow on the topography, small changes occur on the local incidence angle. These small perturbations on wave refraction due to the growing bars (and also to the currents) have been neglected. In our opinion, this could be the main limitation of the present study since recent research by *Caballeria et al.* [2002] showed that wave refraction is essential for the growth of shore-normal bars in case of shore normal wave incidence. Consistently, this type of bars are not obtained in the present model. However, that paper also showed that crescentic bars were not affected by wave refraction because of their small cross-shore span in comparison with their alongshore length scale. The two systems just appeared for different parameter values. Similarly, we do not think that refraction has a significant influence for the initial growth of the very oblique down-current oriented bars because they are very elongated with a very small cross-shore span. In contrast, some influence could be expected in case of up-current oriented bars. Including wave refraction effects in the linear stability analysis is not technically straightforward and is left for future research.

[62] Another important assumption refers to the parameterization of sediment transport, related only to the depth averaged current, $\vec{v}$. As already discussed, this makes sense as long as the longshore current and the rip currents are stronger than undertow and the effects of cross-correlation between waves and sediment. As a result, the 3D morphodynamics related to these currents is usually faster than the 2D morphodynamics associated only to the effect of the waves. The different sediment transport modes, characterized by α_m and m in the term $\alpha_m|\vec{v}|^m$ of the sediment flux, have been investigated in isolation. This has allowed to get

better insight on the physical mechanisms that generate each topography. We think that this also provides a general overview of the behavior for more realistic parameterizations including all the powers of $|\vec{v}|$.

[63] Some approximations in the computation of the wave radiation stress tensor have been assumed in this research (see section 2.1): (1) shallow water wave kinematics, $c_g \simeq c \simeq \sqrt{gD}$, (2) small wave incidence angle, (3) regular waves and (4) saturated surf zone, $H = \gamma_b D$ and wave forcing neglected out of the surf zone, $\partial \mathcal{S}'_{ij}/\partial x_j \simeq 0$. Shallow water wave kinematics is a sensible assumption since, for instance, for a typical wave of 8 s of period on 1 m water depth, the first assumption only gives a relative error of 2%. The assumption of small wave incidence angle is not crucial. In case of $\theta_b = 15°$, it produces relative errors of 4, 5 and 10% on $\mathcal{S}'_{11}$, $\mathcal{S}'_{22}$ and $\mathcal{S}'_{12}$, respectively. Even if the model has been forced to larger angles, all the features predicted have already a significant growth rate for moderate angles of about 5–15°. The approximation is considered acceptable in this range. The results of the model for larger incidence angles at the break point (15–35°) have to be considered with care. Notice that these large angles are not very common in nature because waves are strongly refracted in the shoaling zone (see a quantitative example in section 5.1).

[64] Using regular waves (third assumption) is not a real limitation with respect to random waves with a single narrow peak in frequency. In the equilibrium state, it leads to a single break point. All the variables are continuous across the break point and only their gradients can undergo discontinuities. However, this is not crucially different from the strong gradients that are found when waves start breaking even in case of more realistic random wave descriptions. Out of the equilibrium, waves enter the model essentially through the radiation stress, which needs the energy density distribution. The only essential characteristic of this energy distribution for the instability mechanisms described here is a strong decrease in energy inside the surf zone, as waves approach the coast, which is larger on the shoals and weaker at the troughs. This behavior occurs with both regular and random waves.

[65] Ignoring the gradients in radiation stress out of the surf zone and using the saturated surf zone approximation (fourth assumption) is the simplest way to explore the effect of wave breaking as the main driving force of nearshore hydrodynamics and morphodynamics. This assumption does not affect the longshore momentum balance because the combination of a constant cross-shore energy flux with the Snell's law for wave refraction results in $\partial \mathcal{S}'_{yx}/\partial x = 0$ in the shoaling zone. On the other hand, changes in the cross-shore momentum balance due to this assumption are noticeable. For the basic equilibrium, this approximation has only a small effect on the mean water depth because it suppresses the set-down caused by wave shoaling. Taking this set-down into account would just introduce a small correction in the total water depth for the basic state, $D_0(x)$, not larger than about 4%. Out of equilibrium, making this assumption can only affect the crescentic features that grow out of the surf zone, where the gradients in radiation stress, $\partial \mathcal{S}'_{xx}/\partial x$, are proportional to the bathymetric gradients, $\partial D/\partial x$. There are several reasons to suspect that even considering wave forcing in the shoaling zone would not change the crescentic pattern dramatically. A simple computation shows that a given gradient in water depth, $\partial D/\partial x$, produces a gradient in the radiation stress tensor that is about 4 times larger in the surf zone than in the shoaling zone.

[66] The bottom friction used is proportional to the fluid velocity. This assumption is valid for weak currents with respect to the wave orbital motions so it is in principle applicable in case of wave-dominated beaches ($m = 1$). The same linear formula for the bottom friction has been used in case of $m = 3$, 4 although a quadratic friction would be in principle more consistent for current-dominated beaches. The reason for this choice is that the equilibrium basic state used, which is analytical, can only be computed with a linear friction [*Longuet-Higgins*, 1970]. However, some tests have been performed with a quadratic friction in the linearized equations and the resultant topography is the same. Just a slight modification of the growth rates is obtained.

[67] Finally, the validity of using a planar basic topography, $z_b^0(x) = -\beta x$, can be examined. Because of our assumption of "frozen 2D dynamics," checking $q_x(x) = 0$ for the basic topography does not make sense. Thus, any $z_b^0(x)$ profile could be adopted if it is not far from the observed profiles in nature. These tend to be upward concave, but very often with a planar terrace close to the shoreline [*Plant et al.*, 2001]. Therefore, a planar slope with a suitable β is sensible as basic topography. From a hydrodynamic point of view, the essential aspect of our analysis is that the ocean is split between a single surf zone close to the coast and an offshore zone where wave forcing is absent. In this respect, any monotonic beach profile (i.e., decreasing $z_b(x)$) is equivalent. In contrast, a barred basic profile leading to more than one surf zone would be essentially different.

6. Conclusions

[68] The present theoretical study has shown that free instabilities of the topography coupled to the flow in the nearshore provide a possible mechanism for the formation of oblique sand bars. Even though this is in line with previous research by *Hino* [1974] and *Christensen et al.* [1994], the richness of the morphodynamic behavior is much larger than what was foreseen in those earlier studies (see Figure 3).

[69] Essentially, these instabilities lead to the growth of down-current or up-current oriented bars usually migrating downstream. These bars appear in the surf zone, the most common being the down-current oriented, and they are sometimes linked to shoals beyond the break line (similarly to the crescentic pattern with alternating shoals and troughs at both sides of the break line obtained by *Falqués et al.* [2000] for normal wave incidence). In qualitative agreement with available field observations, model results indicate that very oblique down-current oriented bars appear in case of current-dominated beaches, with spacings of several times the surf zone width. When dealing with wave-dominated beaches, bars can be crescentic/down-current oriented or up-current oriented (that are less frequent in the parameter space), with spacings about the surf zone width. This depends on the cross-shore distribution of wave stirring. The dimensional (e-folding) growth time of the bars ranges from a few hours to a few days and it is favored by constant

wave conditions. Migration celerity can be up to tens of meters per day.

[70] The main physical mechanism responsible of bar growth is the positive feedback between the evolving topography and the perturbations thereby caused on the hydrodynamics. These generated hydrodynamic perturbations are due to the effects of the topography on both the longshore current (bed-flow effect) and the incident wave field (bed-surf effect). The model predictions of the wave conditions potentially leading to generation of bar systems are not in disagreement with *Wright and Short* [1984]. High dissipative states correspond to absence of rhythmic features whereas 3D bars occur in intermediate states.

Appendix A: Morphological Timescale

[71] An estimate of the dimensional values of the growth time and migration celerity can be obtained by account of the timescale, $T_m = \beta X_b^2/Q$, used to make the governing equations nondimensional, where Q is the order of magnitude of the sediment transport flux ($m^2\ s^{-1}$). An estimate of Q can be obtained by using Bailard's parameterization for suspended load in case of weak current

$$Q \sim 0.01 \frac{c_d}{g\, w_s} U_o^3 U, \tag{A1}$$

where U_o is the scale for the orbital velocity, U the scale of the longshore current and w_s the fall velocity of the sediment. The coefficient in front of this expression comes from the suspended load efficiency divided by the sediment relative density and the porosity term. An estimate of the wave orbital velocity is obtained from shallow water approximation, $U_o \sim 0.5\sqrt{gD}$. Longuet-Higgins solution for the longshore current gives $U \sim (\beta/c_d)\sqrt{gH_b}\ \sin\theta_b$ so that

$$Q \sim 5 \times 10^{-4} \frac{\beta g}{w_s} H_b^2 \sin\theta_b. \tag{A2}$$

In case of strong current, U_o^3 has to be replaced by U^3 in equation (A1) and an expression which is similar to equation (A2) results but with the right-hand side multiplied by $8(\sin\theta_b\beta)^3/c_d^3$. This can lead to a larger Q by a factor of 10.

[72] As a general estimate we will use equation (A2) to obtain

$$T_m = 2 \times 10^3 \frac{w_s}{g\beta^2 \sin\theta_b}\ , \tag{A3}$$

having in mind that in case of current-dominated beaches this would be multiplied by $c_d^3/8(\sin\theta_b\beta)^3$. So the morphological time can be about a factor 10 smaller in this case. Another important effect of dealing with strong current is that increasing friction (c_d) clearly leads to smaller timescales. The system of very oblique down-current oriented bars found in the strong current limit (section 3.1) displays a nondimensional growth rate increasing with friction. This effect is counteracted by the decrease of the timescale with c_d. The final dimensional growth times turn out to be quite independent of friction. Other consequences of equation (A3) are that finer sediment (w_s smaller) gives shorter times but this is usually related to gentler equilibrium slopes (β smaller) so that the resulting trend is not clear. It is remarkable that the magnitude of the morphological time does not depend on the wave height. However, higher waves tend to cause gentler equilibrium slopes and, indirectly, larger morphological time. The most clear trend of equation (A3) is the decrease of timescale by increasing the incidence angle. As a representative case, we can look at a beach of $\beta = 0.01$ built up of sediment with $d = 0.1$ mm for which the fall velocity would be $w_s \simeq 0.01\ ms^{-1}$. For waves with $\theta_b = 5°$ the morphological timescale would be of about 64 h. For more oblique wave incidence, this would become some 7 h. In case of a beach slope of $\beta = 0.05$ and $d = 0.3$ mm morphological timescales 5 times shorter would be obtained. As the growth rates computed with the model are of order 1 (except for very small angle in case $m = 1$), typical values of the growth time, $\omega_i^{-1} T_m$, are given by T_m.

[73] From the morphological time, the estimate of the migration speed follows

$$V_{mi} = c\frac{X_b}{T_m} = 5 \times 10^{-4}\, c\, \beta \frac{gH_b}{w_s} \sin\theta_b. \tag{A4}$$

Notice that the same estimate can be obtained as well from the advection term of the linear BEE equation (8), $m\alpha V^m/D_0$. Thus, V_{mi} increases with H_b and θ_b, which makes sense. In the first case discussed above, ($\beta = 0.01$, $d = 0.1$ mm and $\theta_b = 5°$) this leads to 38 m/day for waves of $H_b = 1$ m, assuming that c is order 1. In the same case with very oblique incidence the migration would be about 10 times faster. However, this gives only an estimate of the maximum celerity, by assuming $c \sim 1$, which is usually the case. Yet we should recall that c can be smaller and even zero or negative (stationary topographic pattern or upflow migrating).

Appendix B: Results for Nearly Normal Wave Incidence

[74] The results of our model in case of very small wave incidence angle ($\theta_b < 2–3°$) have not been described in detail on the main body of the paper. There is instability only in case of wave-dominated beaches ($m = 1$) with nonuniform stirring (see Figure 3). Two types of solutions are found, one migrating upflow (mode A1), the other downflow (mode B1). This can be seen in the phase celerity shown in Figure 11. These graphs also show that in case of $\theta_b \rightarrow 0$ the wave number tends to $\kappa_M \simeq 4$. Both modes can be described as crescentic features (alternating shoals and troughs at both sides of the break line). Mode A1 displays elongated inner shoals with the shape of down-current oriented bars whereas the inner shoals of mode B1 are up-current oriented bars (see Figure B1). Figure B2 shows the dispersion line and growth rate curve for $\theta_b = 1°$.

[75] In order to understand these results, it is convenient to recall the solution found in case of normal wave incidence [*Falqués et al.*, 2000]. The "crescentic pattern" described in that paper was stationary. Further unpublished studies using the model for normal wave incidence have demonstrated that, in addition to that stationary solution,

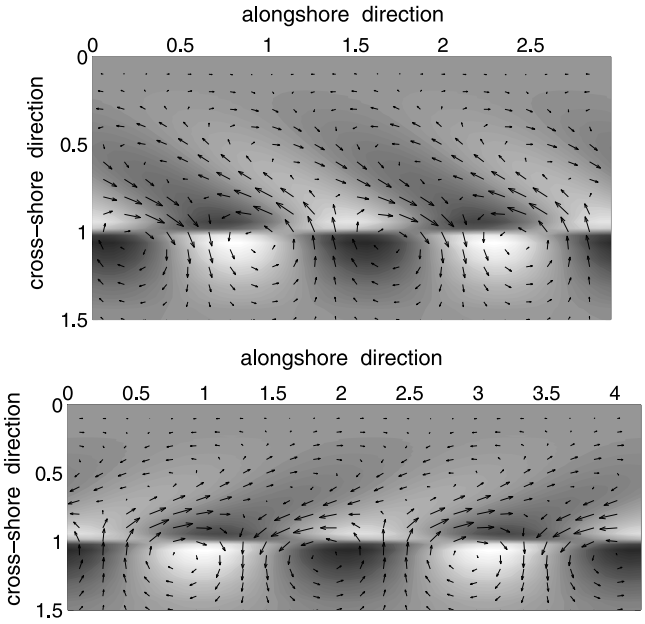

Figure B1. Migrating crescentic bars. Topographic and current perturbations corresponding to the maximum wave number of the mode A1 (top) and mode B1 (bottom) in case of $m = 1$, $\alpha \sim D^2$ and $\theta_b = 1°$. The graph description is the same as in Figure 10.

alongshore migrating solutions may also exist. They appear in pairs, each one migrating with the same celerity but in opposite directions. The solution that migrates in the positive (negative) y-axis direction will be referred to as mode B (A) because of its similarity with the mode B1 (A1) in case of small wave incidence angle. The nonmigrating crescentic pattern will be referred to as mode C. The three solutions have a similar crescentic shape. Figure B3 shows the growth rate and dispersion curves in case of exact normal wave incidence for a particular set of beach and wave parameters. The three solutions A, B and C are shown. Modes A and B have the same growth rates and their maximum wave number is about $\kappa_M \simeq 3.5$, very similar to the result found in case of small wave incidence angle (modes A1 and B1 in Figure B2). Their shape is not shown as it is also very similar to the modes A1 and B1 shown in Figure B1. Mode C does not migrate, $w_{rM} = 0$. An interesting finding is that this nonmigrating pattern has not been recovered in case of small incidence angle. This is certainly due to the symmetry-breaking produced by the

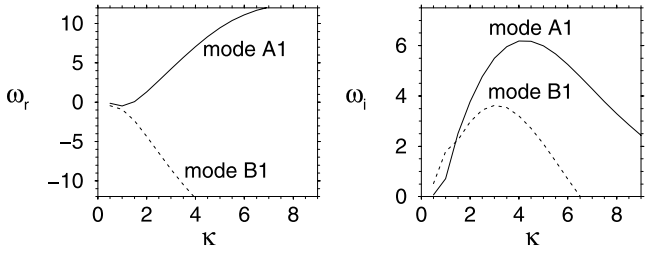

Figure B2. Dispersion line and growth rate curve for $m = 1$, $\alpha \sim D^2$ and very small wave incidence angle. Parameter values are: $\theta_b = 1°$, $r = 0.5$, $\gamma_b = 0.8$, $\gamma = 1$ and $N = 0.01$. As it can be seen, $\kappa_{MA1} = 4.25$, $\omega_{iMA1} = 6.2$ and $\omega_{rMA1} = 7.7$.

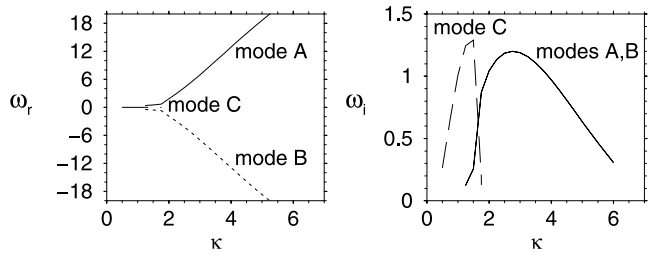

Figure B3. Dispersion line and growth rate curve for $m = 1$ and $\alpha \sim D^2$ in case of normal wave incidence, $\theta_b = 0$, and a particular set of beach and wave parameters.

obliqueness of wave incidence and has an important consequence for morphodynamic instabilities in case of exact normal wave incidence since some of the solutions might be physically unrealistic.

[76] **Acknowledgments.** This research is part of the E.U. funded project SASME under contract MAS3 CT97-0081. F.Ribas thanks the Generalitat de Catalunya for her FI/FIAP grant. Partial funding from the Spanish DGESIC under contract PB98-0929 and the E.U. project HUMOR (EVK3-CT-2000-00037) is also gratefully acknowledged. We also wish to thank Suzanne J.M.H. Hulscher (University of Twente), Aart Kroon (University of Utrecht) and the two anonymous reviewers for their attentive reading and useful comments on the manuscript.

References

Bailard, J. A., An energetics total load sediment transport model for a plane sloping beach, *J. Geophys. Res.*, *86*, 10,938–10,954, 1981.

Barcilon, A. I., and J. P. Lau, A model for formation of transverse bars, *J. Geophys. Res*, *78*, 2656–2664, 1973.

Caballeria, M., G. Coco, A. Falqués, and D. A. Huntley, Self-organization mechanisms for the formation of nearshore crescentic and transverse sand bars, *J. Fluid Mech.*, *465*, 379–410, 2002.

Calvete, D., A. Falqués, H. E. de Swart, and M. Walgreen, Modelling the formation of shoreface-connected sand ridges on storm-dominated inner shelves, *J. Fluid Mech.*, *441*, 169–193, 2001.

Camenen, B., and P. Larroude, Nearshore and transport modelling: Application to Trucvert Beach, paper presented at IAHR symposium, River, Coastal and Estuarine Morphodynamics, Int. Assoc. for Hydraul. Res., Delft, Netherlands, 1999.

Chappel, J., and I. G. Eliot, Surf-beach dynamics in time and space–An Australian case study, and elements of a predictive model, *Mar. Geol.*, *32*, 231–250, 1979.

Christensen, E., R. Deigaard, and J. Fredsoe, Sea bed stability on a long straight coast, in *Coastal Engineering 1994*, vol. 4, edited by B. L. Edge, pp. 1865–1879, Am. Soc. of Civ. Eng., Reston, Va., 1994.

Deigaard, R., N. Droonen, J. Fredsoe, J. H. Jensen, and M. P. Jorgesen, A morphological stability analysis for a long straight barred coast, *Coastal Eng.*, *36*, 171–195, 1999.

Dodd, N., J. Oltman-Shay, and E. B. Thornton, Shear instabilities in the longshore current: A comparison of observation and theory, *J. Phys. Oceanogr.*, *22*, 62–82, 1992.

Evans, O. F., The classification and origin of beach cusps, *J. Geol.*, *46*, 615–627, 1938.

Falqués, A., Formación de topografía rítmica en el Delta del Ebro, *Rev. Geofis.*, *45*, 143–156, 1989.

Falqués, A., V. Iranzo, and A. Montoto, Resonance of longshore currents under topographic forcing, *Phys. Fluids A*, *5*, 3071–3084, 1993.

Falqués, A., A. Montoto, and V. Iranzo, Bed-flow instability of the longshore current, *Cont. Shelf Res.*, *16*, 1927–1964, 1996.

Falqués, A., G. Coco, and D. A. Huntley, A mechanism for the generation of wave-driven rhythmic patterns in the surf zone, *J. Geophys. Res.*, *105*, 24,071–24,088, 2000.

Guilcher, A., A. Godard, and E. Visseaux, Les cretes et sillons obliques de l'estran des Landes de Gascogne, *Com. Oceanogr. Etudes Cotes Bull.*, *4*, 151–157, 1952.

Hino, M., Theory on formation of rip-current and cuspidal coast, in *Coastal Engineering 1974*, pp. 901–919, Am. Soc. of Civ. Eng., Reston, Va., 1974.

Holman, R. A., and A. J. Bowen, Bars, bumps, and holes: Models for the generation of complex beach topography, *J. Geophys. Res.*, *87*, 457–468, 1982.

Horikawa, K., *Nearshore Dynamics and Coastal Processes*, Univ. Tokio Press, Tokyo, 1988.

Hulscher, S. J. M. H., Tidal-induced large-scale regular bed form patterns in a three-dimensional shallow water model, *J. Geophys. Res.*, *101*, 20,727–20,744, 1996.

Hunter, R. E., H. E. Clifton, and R. L. Phillips, Depositional processes, sedimentary structures, and predicted vertical sequences in barred nearshore systems, Southern Oregon coast, *J. Sediment. Petrol.*, *49*, 711–726, 1979.

Konicki, K. M., and R. A. Holman, The statistics and kinematics of transverse bars on an open coast, *Mar. Geol.*, *169*, 69–101, 2000.

Lippmann, T. C., and R. A. Holman, The spatial and temporal variability of sand bar morphology, *J. Geophys. Res.*, *95*, 11,575–11,590, 1990.

Longuet-Higgins, M. S., Longshore currents generated by obliquely incident sea waves, *J. Geophys. Res.*, *75*, 6778–6801, 1970.

Niederoda, A. W., and W. F. Tanner, Preliminary study on transverse bars, *Mar. Geol.*, *9*, 41–62, 1970.

Pattiaratchi, C., and M. Collins, Mechanisms for linear sandbank formation and maintenance in relation to dynamical oceanographic observations, *Prog. Oceanogr.*, *19*, 117–156, 1987.

Phillips, O. M., *The Dynamics of the Upper Ocean*, Cambridge Univ. Press, New York, 1977.

Plant, N. G., B. G. Ruessink, and K. M. Wijnberg, Morphologic properties derived from a simple cross-shore sediment transport model, *J. Geophys. Res.*, *106*, 945–962, 2001.

Ribas, F., A. Falqués, and A. Montoto, Normal mode analysis of the surf zone morphodynamics, in *Coastal Engineering 2000*, edited by B. L. Edge, pp. 3229–3242, Am. Soc. of Civ. Eng., Reston, Va., 2000.

Roelvink, J. A., and M. J. F. Stive, Bar-generating cross-shore flow mechanisms on a beach, *J. Geophys. Res.*, *94*, 4785–4800, 1989.

Ruessink, B. G., I. M. J. Enckevort, K. S. Kingston, and M. A. Davidson, Analysis of observed two- and three-dimensional nearshore bar behaviour, *Mar. Geol.*, *169*, 161–183, 2000.

Schielen, R. R., A. Doelman, and H. E. de Swart, On the dynamics of free bars in straight channels, *J. Fluid Mech.*, *252*, 325–356, 1993.

Short, A. D., *Handbook of Beach and Shoreface Morphodynamics*, John Wiley, New York, 1999.

Sonu, C. J., Collective movement of sediment in littoral environment, in *Coastal Engineering 1968*, pp. 373–400, Am. Soc. of Civ. Eng., Reston, Va., 1968.

Wright, L. D., and A. D. Short, Morphodynamic variability of surf zones and beaches: A synthesis, *Mar. Geol.*, *56*, 93–118, 1984.

A. Falqués, A. Montoto, and F. Ribas, Departament de Física Aplicada, Edifici B4/B5 Campus Nord, Universitat Politècnica de Catalunya, c/ Jordi Girona 1-3, 08034, Barcelona, Spain. (falques@fa.upc.es; amadeo.montoto@upc.es; cesca@fa.upc.es)